



HAL
open science

Interactions of hydrogen with zirconium alloying elements and oxygen vacancies in monoclinic zirconia

Emile Haurat, Marc Tupin, Jean-Paul Crocombette

► **To cite this version:**

Emile Haurat, Marc Tupin, Jean-Paul Crocombette. Interactions of hydrogen with zirconium alloying elements and oxygen vacancies in monoclinic zirconia. *Acta Materialia*, 2022, 225, pp.117547. 10.1016/j.actamat.2021.117547 . cea-03885931

HAL Id: cea-03885931

<https://cea.hal.science/cea-03885931>

Submitted on 6 Dec 2022

HAL is a multi-disciplinary open access archive for the deposit and dissemination of scientific research documents, whether they are published or not. The documents may come from teaching and research institutions in France or abroad, or from public or private research centers.

L'archive ouverte pluridisciplinaire **HAL**, est destinée au dépôt et à la diffusion de documents scientifiques de niveau recherche, publiés ou non, émanant des établissements d'enseignement et de recherche français ou étrangers, des laboratoires publics ou privés.

Interactions of hydrogen with zirconium alloying elements and oxygen vacancies in monoclinic zirconia

Emile Haurat (a), Jean-Paul Crocombette (a) and Marc Tupin (b)

(a) *DES-Service de Recherche en Métallurgie Physique, CEA, Université Paris-Saclay, F-91191 Gif-sur-Yvette Cedex, France*

(b) *DES-Service d'Etudes des Matériaux Irradiés, CEA, Université Paris-Saclay, F-91191, Gif-sur-Yvette, France*

Abstract

Using Density Functional Theory with hybrid functionals, we calculate the interactions of hydrogen atoms with some point defects in monoclinic zirconia. We consider Nb and Sn substitution for Zr atoms as well as oxygen vacancies, the latter being the main defects present in the zirconia layer. They are formed during the corrosion of zirconium claddings in pressurized water reactors. We consider various charges for the complexes formed by hydrogen atoms and the aforementioned defects. The formation and binding energies are thus expressed as functions of the Fermi level in zirconia. We find that there is almost no interaction between H and Sn atoms, while a small but noticeable binding exists between H and Nb atoms. Conversely, hydrogen atoms bind strongly to oxygen vacancies which can accommodate up to 2 hydrogen atoms. We observe that there is a range of Fermi levels where the actual stable form of hydrogen is the H₂ molecule and not isolated hydrogen ions. We integrate the calculated energies in a thermodynamical model to calculate the concentrations of the various forms of hydrogen. We observe that the driving parameters are the oxygen vacancy to hydrogen ratio and the temperature. There is a change in the main stable hydrogen species upon decrease of the vacancy concentration from hydrogen trapped in vacancies to interstitial forms of hydrogen. These results provide a possible rationale for the variation of hydrogen diffusion coefficient through the oxide layer observed experimentally in literature.

I Introduction

In nuclear Light Water Reactors, zirconium alloy fuel claddings are oxidized by primary water. During the corrosion process, the cladding also absorbs a fraction of hydrogen produced by water reduction. When hydrogen concentration exceeds the solubility limit, zirconium hydrides precipitate in the cladding leading to possible embrittlement. Furthermore, during transport or storage of used nuclear fuels, in addition to this embrittlement, the hydrogen accumulated within the cladding is then susceptible to desorb from it, which can involve safety concerns.

All processes, absorption, desorption or hydrogen release, involve hydrogen diffusion through the oxide layer, which is usually considered as the rate-limiting step of these phenomena. In the literature the hydrogen diffusion coefficient through the oxide has been measured using various techniques and protocols. However, values of the diffusion coefficient of hydrogen are very scattered. Indeed, they spread from 10^{-13} to 10^{-17} $\text{cm}^2 \text{ s}^{-1}$ (at 600K). This striking range is mainly due to (i) the difference of experimental techniques used (ii) the fact that the physico-chemical processes studied differ from one study to another. Sometimes one works in absorption, while others work in desorption or in release. Consequently the type of hydrogen species diffusing through the oxide vary depending on the process under study [1-9].

Furthermore the transport properties within the oxide layer are not homogeneous. It is indeed well known that the oxide layer is divided into two sub-layers with different hydrogen diffusion coefficients transport properties [7, 10]. Atom Probe Tomography analysis revealed also that grain boundaries are significantly enriched in hydrogen compared to the volume of the grains [11-13]. Recent works highlighted that the hydrogen fraction within the grain boundaries is around 70% in the middle of the oxide layer [12]. Others evidenced by Transmission Electron Microscopy the presence of nanopores in the oxide [14] and the increase in their density when the oxide grows [15]. According to these authors, the microstructure evolution could explain the variations of hydrogen pickup by the cladding. Hu et al [14] contemplate molecular hydrogen diffusion through the pores while Couet et al. [15] advocate proton migration under an electric field opposite to the move of hydrogen.

Eventually, hydrogen diffusion mechanism in the oxide film is not actually identified and, as a consequence, apparent hydrogen diffusion coefficient is very difficult to assess accurately from experiments. Fundamental calculations can bring relevant help to make progress on this issue.

In a previous study [16], we tackled the insertion of atomic hydrogen in defect-free monoclinic zirconia. We confirmed that atomic hydrogen is a negative U impurity, i.e. hydrogen atoms are ionized, with H^+ or H^- ions stable, depending on the position of the Fermi level in the gap. We explored in details the stability sites of the hydrogen ions and the migrations between them. We found that the energetic

landscape of these ions in zirconia is quite complex, especially for protons. We eventually obtained the diffusion coefficients of atomic hydrogen in ZrO_2 . The diffusion of protons proves orders of magnitude faster than that of hydride ions. However, the diffusion coefficients for protons we calculated are 7 orders of magnitude larger than the values deduced from experiments even if those are very scattered. Such a large discrepancy cannot be accounted for solely by electric field effects. The irradiation-free oxidation process of zirconium alloys takes place according to an inner oxide growth mechanism which involves the diffusion of oxygen vacancies produced at the metal/oxide interface. These defects are therefore likely to interact with hydrogen.

In the present study, we tackled the possible trapping of hydrogen onto point defects in zirconia. We use the same theoretical framework as before: Density Functional Theory (DFT) calculations at the atomic scale (see section II). The point defects we are dealing with are on one hand oxygen vacancies, and on the other hand tin (Sn) or niobium (Nb) substitutional atoms for zirconium. The latter are the main alloying elements in the major nuclear zirconium alloys for claddings. For the sake of completeness, we also studied the possibility to insert H_2 molecules in interstitial positions in zirconia. Calculated energies are integrated in a thermodynamic model to estimate the relative population of hydrogen sites as a function of temperature, hydrogen content and oxygen vacancies concentration.

II Technicalities

II.1 DFT Calculations

We use the same theoretical framework as in our previous study [16] on atomic hydrogen in zirconia, to which the reader is referred for details. We performed DFT calculations using the VASP (Vienna *Ab initio* Simulation Package) code [17, 18], in the Projector Augmented Wave framework [19]. For each defect the structure is pre-relaxed with the PBE Generalized Gradient Approximation [20] and further relaxed with HSE06 hybrid functional [21] down to forces lower than $0,02\text{eV}/\text{\AA}$. Only the hybrid functional results are shown. Our basic simulation box is a $2*2*2$ supercell of the 12 atom zirconia unit cell. Calculations are performed at the Γ point. *We checked on some test configurations the effect of box size. The formation energies (equations 2 to 4, below) in $3*3*3$ boxes are different by around +/- 0.05eV from the ones of $2*2*2$ boxes. Such a small energy difference does not alter our qualitative conclusions.* We studied the following point defects: Sn or Nb substitution of zirconium atoms and oxygen vacancies. For the latter, two inequivalent positions exist in the structure: one with three Zr atoms around each oxygen and one with four. Both positions are systematically considered. For the substitutional defects we calculated boxes containing a hydrogen atom in various

positions close to the atoms in substitution. For oxygen vacancies, one, two or three hydrogen atoms are introduced in the vacancy (again testing various atomic arrangements). All these point defects or defect complexes may be charged. We therefore calculated their energy of boxes with the addition or removal of electrons. The electrons or holes are simply added to the box, they are not forced to localize on the defect. If the defect can indeed be charged these additional electrons or holes will localize around the defect and defect levels will appear in the band gap. In the following when we mention the “charge of the defect”, we are in fact referring to “the charge of the box which contains the defect”. Thus, these charges should not be confused with the actual charges of the atoms forming the defects. The complete list of defects under study is as follows.

Defects and impurities: V_O^q with charge q from -1 to +2; Sn_{Zr}^q ($q = -2, -1, 0, +1$), formally corresponding to valences Sn^{2+} to Sn^{5+} ; Nb_{Zr}^q ($q = -1, 0, +1$), formally corresponding to valences Nb^{3+} to Nb^{5+} . Hydrogen interstitials in atomic H_i^q ($q = -1$ to +1) or molecular form H_{2i}^q ($q = -2$ to +2). Hydrogen in oxygen vacancies H_O^q ($q = -1$ to +3), $(2H)_O^q$ ($q = -2$ to +4), and $(3H)_O^q$ ($q = -3$ to +5). Hydrogen atoms close to substitutional atoms $(H - Sn_{Zr})^q$ ($q = -2$ to +2), $(H - Nb_{Zr})^q$ ($q = -2$ to +2), and $(H_2 - Nb_{Zr})^q$ ($q = -3$ to +3). Boxes with an odd number of electrons are calculated with spin-polarized calculations. Boxes with an even number of electrons are generally calculated with a non spin-polarized set-up. We checked on a few boxes that for an even number of electrons, the energies with or without spin polarization are essentially equal.

11.2 Energies

From the raw energies of the relaxed simulation boxes ($E(D^q)$ for defect D of charge q), one can calculate various formation or reaction energies. The first step is to correct the energies of charged boxes and include their dependence on the value of the Fermi level. One then obtains the corrected energies of the boxes containing defects $\tilde{E}(D^q)$. The variation with the Fermi level is kept apparent.

$$\tilde{E}(D^q) + q\epsilon_F = E(D^q) + q(\epsilon_F + \epsilon_{BV}) + \frac{q^2\alpha_M}{2\epsilon L} \quad (1)$$

In this equation, ϵ_{BV} is the VASP energy of the top of the valence band in the defect free supercell and ϵ_F is a parameter indicating the energy of the Fermi level measured from the top of the valence band. The last term is the major correction of the energies of charged boxes [22]. It depends on the Madelung constant of the structure (α_M calculated by VASP), the size of the box (L), and the dielectric constant of the material for which we take the 23 experimental value [23]

From these $\tilde{E}(D^q)$ we use two different sets of equations. First, the formation energy of each point defect or defect complex, which is written as a function of the chemical potentials of its constituents.

The most simple example is the formation energy of an oxygen vacancy of charge q which depends linearly on the chemical potential of oxygen (μ_O) and ϵ_F :

$$E^f(V_O^q) = \tilde{E}(V_O^q) + q\epsilon_F - E(ZrO_2) + \mu_O = \Delta\tilde{E}(V_O^q) + q\epsilon_F + \mu_O \quad (2)$$

Such an expression is written for each possible charge state of the oxygen vacancy with the energy of the corresponding box. $E(ZrO_2)$ is the VASP energy of a 96 atom defect free zirconia box, which balances the equation in terms of number of Zr and O atoms. For more complex defects, such as hydrogen-vacancy or hydrogen-substitution complexes, the expressions involve the chemical potentials of the various constituents of the defect. For instance in the case of one hydrogen atom in an oxygen vacancy, one has:

$$E^f(H_O^q) = \Delta\tilde{E}(H_O^q) + q\epsilon_F + \mu_O - \mu_H \quad (3)$$

In the same way, for a substitution, one has (e. g. for Nb):

$$E^f(Nb_{Zr}^q) = \tilde{E}(Nb_{Zr}^q) + q\epsilon_F - \frac{31}{32}E(ZrO_2) - 2\mu_O - \mu_{Nb} \quad (4)$$

For now, the chemical potentials of Nb and O are arbitrarily fixed at the energy of the isolated atoms, which are fixed by definition to 0 in VASP (see section IV for a calculation of the actual values of these potentials). One then obtains a set of linear expressions for the energies as a function of the Fermi level. See figure 1 for the case of formation energies of oxygen vacancies for the various charge states. The lines cross at the so-called Charge Transition Levels (CTLs). Equivalent expressions can easily be written for any defect cluster. They will be intensively used in the thermodynamic modelling of section IV.

For any specific ϵ_F , one may also consider the minimum among the different charges of the energies:

$$\bar{E}(V_O) = \min_q(\Delta\tilde{E}(V_O^q) + q\epsilon_F) \quad (5)$$

For any Fermi level, this simply corresponds to the lowest energy among the various lines. \bar{E} energies are concave piecewise linear functions of the Fermi level.

Second, to calculate the energy gain upon binding of hydrogen to defect, we use the reaction energy with respect to the atomic hydrogen interstitial. As an example, the binding energy of an interstitial hydrogen to an oxygen vacancy comes from the reaction:



In principle, this reaction should be written for all possible charge states of the various components of the reaction: atomic interstitial hydrogen, oxygen vacancy, and H_O . However, in order to ease the

presentation, we show in subsequent figures, for any specific Fermi level and defect, the charge of minimum energy:

$$E^b(H_O) = \bar{E}(H_O) + E(ZrO_2) - \bar{E}(H_i) - \bar{E}(V_O) \quad (7)$$

One then obtain piecewise linear reaction energies as a function of the Fermi level (see fig 2 and 3) with slope change for each of the CTLs of the Right Hand Side terms of the equation 7. In these graphics, a negative reaction energy denotes an energy gain (a binding) upon association of the interstitial hydrogen(s) with the vacancy or impurity.

III Results

III.1 Defect sites without hydrogen

Formation energies (E^f) of oxygen vacancies and Nb or Sn substitutional impurities are shown in **Erreur ! Source du renvoi introuvable.** One can see that the oxygen vacancy goes from +2 to neutral with the increase of the Fermi level in the gap. A very tight domain of stability of +1 charge is in between. Sn in substitution for a zirconium atom are preferentially neutral except for the Fermi levels close to the conduction band where its effective charge state is -2 (corresponding to Sn^{2+}). The valence of Sn ions in zirconia is thus mostly the same as that of zirconium. At the opposite, boxes with Nb in substitution for a zirconium atom are +1 charged for most of the gap with small range of 0 then -1 stability after a 4eV CTL. In valence terms, Nb thus proves to be mainly +V or +III depending on the position of the Fermi level, at odds with the +IV value for Zr. The present results are very comparable to the ones obtained by Bell et al [24] on their study of the possible valence of Nb in zirconia. These charge states are consistent with experimental data, especially, for +V oxidation state with X-rays Photoemission Spectroscopy analysis performed on the surface of the oxide film [25, 26] and for +III charge state with XANES experiments showed that niobium oxidized for thermodynamic reasons with delay compared to the α -Zr matrix [27]. For tin, in agreement with our calculations, Mossbauer spectroscopy carried out on oxide layers grown in Zircaloy-4 [28] revealed Sn^{4+} and Sn^{2+} in the oxide, which can be related to the stable boxes with charges 0 and -2 respectively .

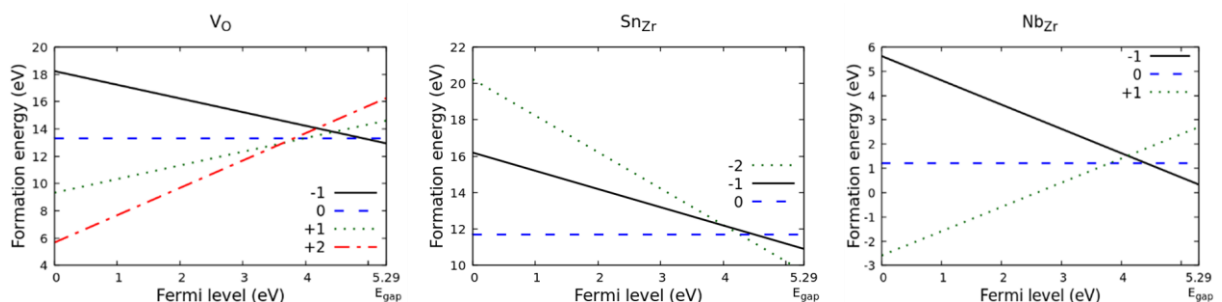


Figure 1: Formation energy of defect sites in monoclinic zirconia for various charges as a function of Fermi level (see text for details).

III.2 Hydrogen in oxygen vacancies

The charge of the complex formed by a hydrogen atom inside an oxygen vacancy is always positive for almost ϵ_F , see Figure 2.

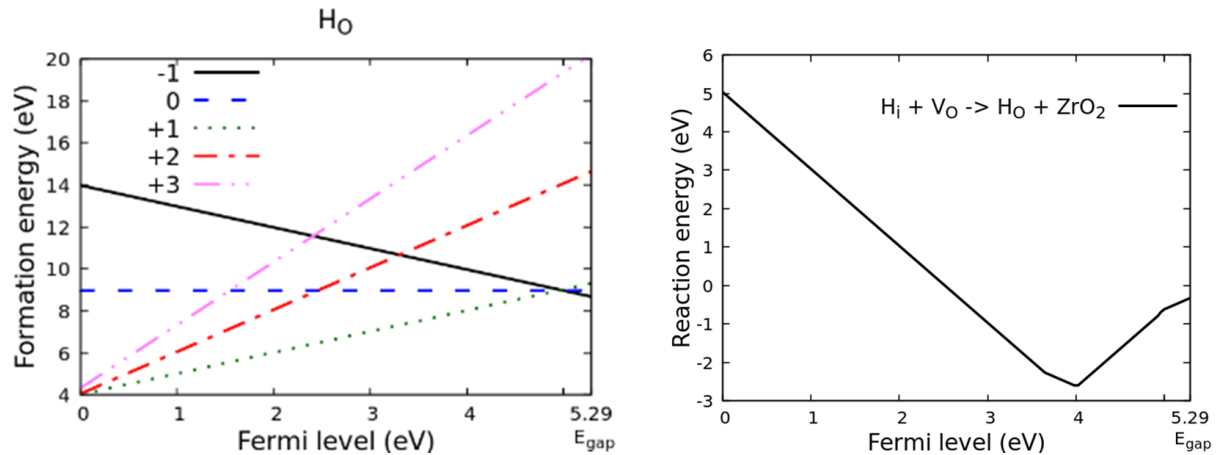


Figure 2: Energies of one hydrogen atom in an oxygen vacancy. Left panel: formation energies for various charges of the H₀ complex as a function of the Fermi level. Right panel: reaction energy to form the H₀ complex from an oxygen vacancy and an interstitial hydrogen as a function of the Fermi level (Eq 7).

Reaction energies of an interstitial hydrogen going into an oxygen vacancy is shown on the right side of Figure 2. In the first two thirds of the gap the reaction energy decreases steeply going from strong repulsion ($\epsilon_F < 2.5$ eV) to strong attraction with a slight plateau just before $\epsilon_F = 4$ eV. At this point, the binding energy is quite large. Indeed, 2.5 eV is gained upon association of a hydrogen interstitial with an oxygen vacancy. Upon further increase of the Fermi level, the reaction energy re-increases but the binding remains favourable up to the conduction band.

Hydrogens are more stabilized in the vacancies formed by trivalent oxygen sites than those formed by tetravalent ones. When the hydrogen is trapped in the vacancy, it is about 0.05 Å away from the initial oxygen position. The distortion due to the hydrogen presence is thus quite small.

The association of an additional hydrogen to an already existing H₀ complex proves less energetic (see figure 3). Its reaction energy profile exhibits two plateaus of moderate interaction energies. A +0.8 eV reaction energy for the first half of the gap indicates the instability of an additional H in the vacancy in this range. At the opposite, between $\epsilon_F = 4$ and 5 eV, 0.6 eV is gained upon a second hydrogen binding. The energy gain around 4 eV thus proves much lower for the association of a second hydrogen than for the first binding of H to V_O.

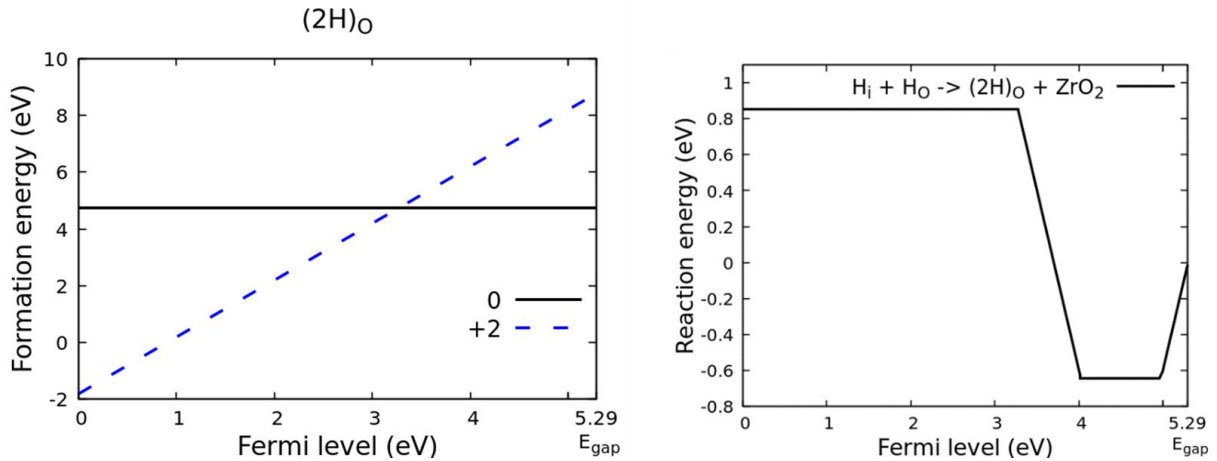


Figure 3: Energies of two hydrogen atoms in an oxygen vacancy. Left panel: formation energies for various charges of the $(2H)_O$ complex as a function of the Fermi level. Right panel: reaction energy to form the $(2H)_O$ complex from a H_o complex and an interstitial hydrogen as a function of the Fermi level.

We tested the possibility to bind a third hydrogen atom to an oxygen vacancy. It turns out that such configurations are always energetically unfavourable. We do not consider them any further in this study.

Looking at the atomic positions of the H atoms inside the vacancies, we noted that the first hydrogen is positioned close to the emptied oxygen position. When present, the second hydrogen lies rather at the periphery of the vacant site, close to an existing interstitial site. The distance between the two hydrogen atoms is too large (2.0\AA) to consider they form a H_2 molecule. It looks more like one hydrogen trapped in the vacancy interacts strongly enough with an interstitial one next to it to bring it closer of 0.24\AA .

III.3 H close to substitutional atoms

Binding energies between the hydrogen and the Sn or Nb substitutional atoms are shown in Figures 4 and 5. It appears clearly that the interaction of interstitial hydrogen with Sn atoms is rather weak with binding around 0.21 eV for most of the gap and a repulsion of maximum 0.15 eV for Fermi levels higher than 4.7 eV. The repulsion becomes noticeable only in the last tens of eV close to the conduction band. Sn atoms having mostly the same valence as Zr atoms, their interaction with hydrogen ions is thus very limited. Indeed the H and the Sn atoms experience very small displacements upon relaxation. They remain in their initial positions and are always some 2.5 to 3\AA apart.

Conversely, the distance between H and Nb atoms depends strongly on the charge of the box. For +2 and +1 boxes, H is in an H^+ interstitial position, not interacting with the Nb. For 0 and -1 boxes, H ends up at about 1.75\AA from Nb, close to an H^- interstitial position which is initially at 2.15\AA apart from Nb. They get closer to each other because of their quite strong interaction, as we can see on the right side of Figure 5. For lower Fermi levels there is a small repulsion between the two atoms which turns to a moderate 0.45eV binding between $\epsilon_F=4$ and $\epsilon_F=4.5\text{eV}$. The upper Fermi level sees a rapid increase of the reaction energy, which denotes a rapid shift from moderate binding to strong repulsion as the Fermi level approaches the bottom of the conduction band.

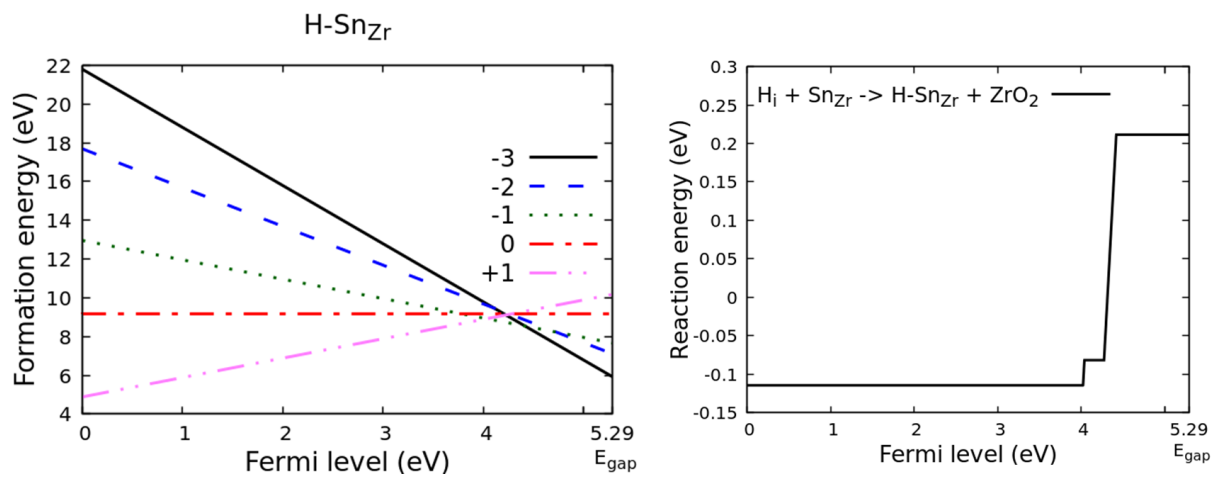


Figure 4: Energies of one hydrogen atom close to a substitutional tin atom. Left panel: formation energies for various charges of the $H-Sn_{Zr}$ complex as a function of the Fermi level. Right panel: reaction energy to form the $H-Sn_{Zr}$ complex from a substitutional Sn_{Zr} atom and an interstitial hydrogen as a function of the Fermi level.

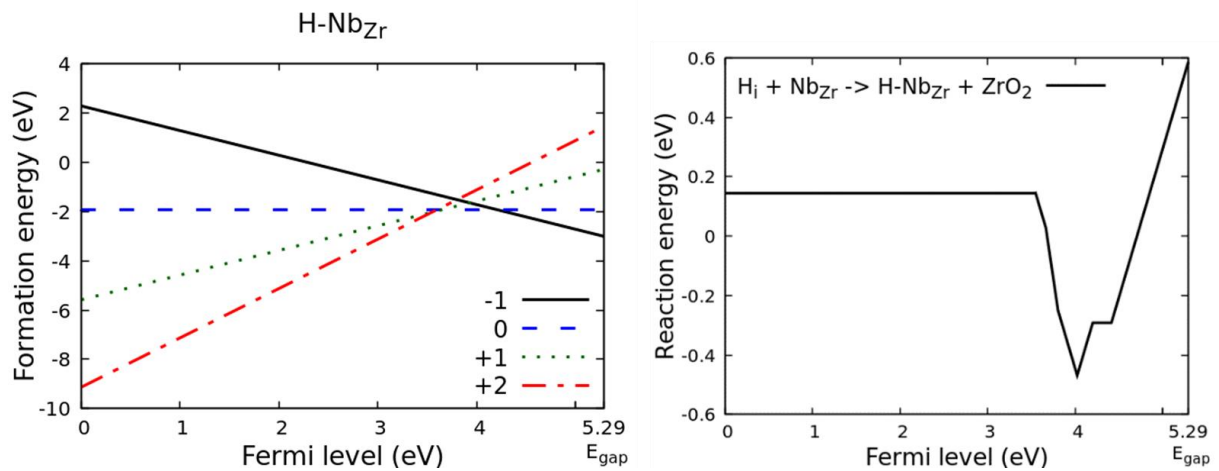


Figure 5: Energies of one hydrogen atom close to a substitutional niobium atom. Left panel: formation energies for various charges of the $H-Nb_{Zr}$ complex as a function of the Fermi level. Right

panel: reaction energy to form the $H\text{-Nb}_{Zr}$ complex from a substitutional Nb_{Zr} atom and an interstitial hydrogen as a function of the Fermi level.

III.4 Stability of molecular hydrogen in zirconia

For the sake of completeness, we calculated the energy of a dihydrogen molecule in interstitial position in zirconia. We positioned the centre of the molecule in the various interstitial ionic hydrogen sites (see our previous study) and oriented the H_2 molecule along each of the a, b and c axis. In the end, H_2 sits in a unique interstitial position. The middle of the molecule isn't close to any atomic interstitial position. The H-H interatomic distance is 0.75\AA , very close to the one of gaseous dihydrogen.

The reaction energy for the association of 2 hydrogen ions into a H_2 molecule is given in the right part of Figure 6. For most of the Fermi levels, this association is unfavourable (with a positive reaction energy). However, for a small ϵ_F interval close to the H+/H- CTL the formation of a H_2 molecule proves energetically favourable. This opens the possibility for the H_2 molecule to be the stable form of interstitial hydrogen in zirconia. This is a rather unexpected result (see the discussion section).

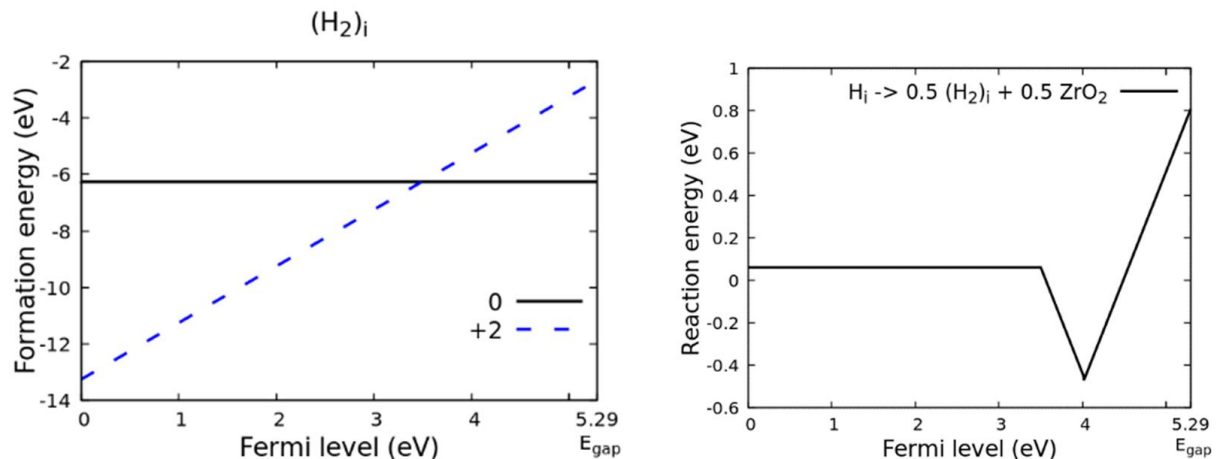


Figure 6: Energies of an interstitial H_2 molecule. Left panel: formation energies for various charges of the H_2 molecule as a function of the Fermi level. Right panel: reaction energy to form the $\frac{1}{2} \text{H}_2$ molecule complex from an interstitial hydrogen as a function of the Fermi level.

As one can see on figures 2 to 6, the binding of interstitial hydrogen to the various defect sites is maximum (lowest reaction energies) around $\epsilon_F = 4$ eV in the gap. This is in fact an energetics effect due to the interstitial hydrogen itself. Indeed, that interstitial hydrogen has its highest energy at its CTL at 3.99 eV in the gap. It is therefore not surprising to obtain more favourable binding around this ϵ_F .

IV Thermodynamic model for the stability of hydrogen in zirconia

IV.1 Presentation of the model

In the previous section, we have shown that there are ranges of Fermi levels for which exists a large energy gain upon binding hydrogens with oxygen vacancies and a slighter gain in the H-Nb_{Zr} association or H₂ molecules formation. The existence of these energy gains does not warrant the actual trapping of hydrogen by these defects. Indeed, the aforementioned energies are negative only in a little portion of the gap. Furthermore, these are just internal energies, which cannot directly translate into actual concentrations of each type of configurations, since they do not take into account temperature effects and especially configuration entropy. To estimate the thermodynamic distribution of H in ZrO₂, we built a model based on the following assumptions: first, point defects and clusters are non-interacting and infinitely diluted; second, entropy effects are neglected beyond simple configuration entropy. This model is a simple extension of the point defect model frequently used to analyse the disorder in oxides, especially UO_{2+x}. [29, 30].

Under these assumptions, one can calculate the concentration of the various defect complexes from their formation energies. For instance, the H_O complex (designed H_O) one has concentration is:

$$[H_O^q] = \exp\left(\frac{-E^f(H_O^q)}{k_B T}\right) = \exp\left(-\frac{\Delta\tilde{E}(H_O^q) + q\epsilon_F + \mu_O - \mu_H}{k_B T}\right) \quad (8)$$

Equivalently for H close to Nb_{Zr}:

$$\begin{aligned} [(H - Nb_{Zr})^q] &= \exp\left(\frac{-E^f((H - Nb_{Zr})^q)}{k_B T}\right) \\ &= \exp\left(-\frac{\Delta\tilde{E}((H - Nb_{Zr})^q) + q\epsilon_F + \mu_{Zr} - \mu_H - \mu_{Nb}}{k_B T}\right) \end{aligned} \quad (9)$$

In view of the weak interactions of H with Sn_{Zr} substitutional atoms, we do not consider them in the following. In these equations, $\Delta\tilde{E}(D^q)$ is a corrected energy in eV extracted from differences of VASP energies. ϵ_F , μ_O , μ_{Zr} and μ_{Nb} are unknown parameters to be determined, T is the temperature of interest and k_B the Boltzmann constant. Equivalent equations can be written for all defect complexes calculated in the previous section. One can still see the dependence of the concentrations on the unknown chemical potentials of the elements and the Fermi level. Note that as the material under study is ZrO₂, the following relationship applies to O and Zr chemical potentials:

$$\mu_{Zr} + 2\mu_O = E(ZrO_2) \quad (10)$$

For given chemical potentials, the concentration of each defect cluster depends solely on the Fermi level. Its value can be assigned by ensuring electroneutrality of the whole crystal which enforces the following condition on the concentrations of defects D^q :

$$\sum_{D,q} q[D_q] = 0 \quad \sum_{D,q} q[D^q] = 0 \quad (11)$$

There is only one Fermi level that gives a zero net charge. Indeed, the global charge is a monotonously decreasing function of the increasing Fermi level starting from the top of the valence band where all defect levels are empty of electrons to the bottom of the conduction band where all defect levels have been filled as the Fermi level successively crosses the various CTLs. Therefore, a given set of chemical potentials and temperature leads to a unique Fermi level which in turn corresponds to a given set of concentrations of the various defect complexes.

The question of the determination of the $\mu_{O'}$, $\mu_{H'}$, and μ_{Nb} chemical potentials remains. These chemical potentials could be estimated from thermodynamic equilibrium with specific reference states. For instance, one could consider zirconia in equilibrium with some specific di-oxygen and di-hydrogen pressure and some specified Nb potential. This is the natural path when one wishes to deal with the equilibrium state in a well-defined thermodynamic situation. For the present study, we have chosen a slightly different path. The technological process we are interested in is the hydrogen uptake concurrent with the corrosion of zirconium alloy in the primary circuit of nuclear reactors. This is a highly non equilibrium situation. Even if one neglects, as we will do in the following, the effect of neutron irradiation on defect populations, corrosion experiments are by design non equilibrium situations. Because of an inward oxide growth process associated to oxygen vacancy diffusion, the oxygen vacancy concentration vary from one side of the oxide layer to the other [31]. One can nevertheless assume some local equilibrium among the various sites of hydrogen for given concentrations of the various species. We thus chose to fix total concentrations of hydrogen, niobium and oxygen vacancies in zirconia and designed a search for the chemical potentials that will give these chosen values. We then have access to the concentrations of the various hydrogen sites in the material.

The Nb concentration in substitution for Zr in the monoclinic zirconia is fixed at the one measured in solid solution in the metal which is around 0.3-0.4 at% [32]. This assumption means that niobium in solid solution in the metal is oxidized concurrently with zirconium upon extension of the oxidation front. Furthermore, using X-ray Absorption Near Edge Structure on oxide layers formed on Zr-0.4%Nb alloy, Couet et al. [31] measured a niobium solid solution concentration of around 0.2 at.%.

The hydrogen concentration in Zr-4 grains is fixed to 0.3 at%. Again, this concentration is a reasonable guess based on ERDA measurements of the hydrogen concentration in the oxide layers (~1 at.%) [7]

combined with SAT analysis on hydrogen distribution between the grain boundaries and the grains [12].

The concentration of oxygen vacancies is much more difficult to establish and, as indicated above, it quite certainly varies from the outer zirconia layer in contact with water to the internal ZrO_2 /zirconium interface. However, Ma et al. made thermodynamic calculations in the range from 720 to 1478K (the phase transition temperature from monoclinic to tetragonal zirconia). The extrapolation of these data leads to an estimation of the sub-stoichiometry at 600 K of a few tenths of percent. We choose to show the results for vacancy concentrations from 0 to 0.4 at% as no further evolution can be observed for higher concentrations. For each vacancy concentration, we search for the chemical potentials and Fermi level that ensure that the total concentrations of Nb, H, and V_O are as specified and the solid is electrically neutral. Technically, this search is expressed in terms of finding the zero of the sum of the square differences between calculated concentrations at a given triplet of chemical potentials and target ones.

This function being highly nonlinear we use a genetic algorithm as implemented in the scipy python package [33] to automate the search. Any vacancy concentration leads to a single set of chemical potential and thus a single set of defect complex concentrations.

The H/V_O ratio proves to be the main drive for the distribution of H among its various sites. So we present the results in figure 7 as a function of the oxygen vacancy concentration for 3 different temperatures, ranking from 600 K to 1400 K to observe the trend at temperatures from normal operation conditions up to the LOss of Coolant Accident (LOCA) conditions.

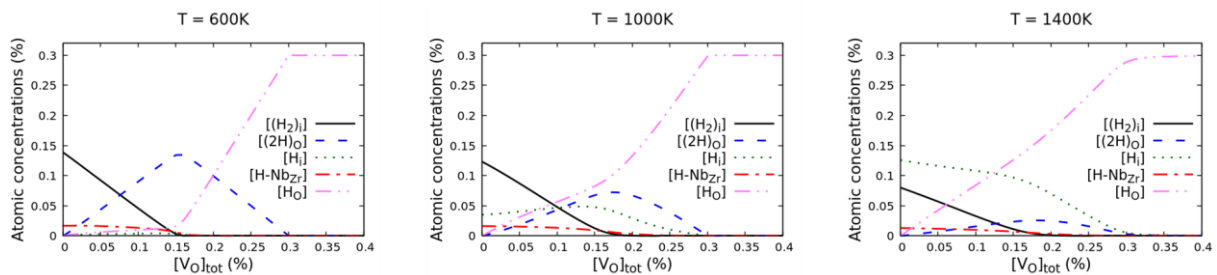


Figure 7: Concentrations of hydrogen in its various sites as a function of the oxygen vacancy concentration for various temperatures. See section IV.1 for the underlying thermodynamic model.

At the lowest temperature, H atoms tend to fill the available sites directly according to their lowest energy. Thus, at high oxygen vacancy concentration, where there is more than one vacancy per H atom, all hydrogen atoms are in the form of H_O , a single hydrogen atom per vacancy. Upon decreasing of vacancy concentration, hydrogen atoms can no longer be all accommodated as single H_O and thus form $(2H)_O$ complexes. At $[H]_{tot}/[V_O]_{tot} = 2$ all vacancies are filled with two hydrogen atoms. Upon further

decrease of the number of vacancies, hydrogen form interstitial H_2 molecules. H^+ or H^- monoatomic interstitials are almost negligible at these temperatures. There is however a residual concentration of such atomic H bounded with Nb atoms. Increasing the temperature triggers the entropy effects which favour the unbound configurations. For the highest temperature (1400 K), mono-hydrogen configurations H^+/H^- and H_o are dominant with H_o favoured for large vacancy concentrations. 1000 K appears as the turning point for which mono and diatomic hydrogen configurations are equally important in the hydrogen distribution. At $[V_o] = 0.1\%$ one can see that the 4 concentrations of H, $(H_2)_i$, H_o , and $(2H)_o$ are almost equal. The insertion of hydrogen is then rather complex with 4 competing sites.

As previously mentioned, the oxide layer formed on zirconium alloys is divided into two sub-layers in the oxide with different hydrogen transport properties [7, 10] [4, 8]. The hydrogen diffusion coefficient ratio between the external part and the inner part of the oxide layer is about two orders of magnitude at 600K, being higher in the external part. Furthermore, a vacancy concentration gradient is built through the oxide layer because of vacancy production at the metal/oxide interface and its consumption at the surface. According to this work, there is a change in the main hydrogen species upon decrease of the vacancy concentration. Supposing that there is effectively 0.4% vacancy concentration at the inner interface at 600K, hydrogens will be trapped in these defects to form (H_o) defects as shown in Figure 7a. However, considering, as usually done, that the oxide is close to the stoichiometry at the surface of the oxide film, the main hydrogen species in this case is molecular hydrogen in interstitial position $(H_2)_i$. It is almost certain that these species don't have the same transport properties and do not diffuse with the same rate. In other words, these results provide a possible explanation for the variation of hydrogen diffusion coefficient through the oxide layer observed experimentally. We are nevertheless aware other interpretations exist. Electric field or microstructure effects should indeed play a role on hydrogen diffusion [14] [15].

V Conclusion

Our results bring new insights on the insertion of hydrogen in monoclinic zirconia. The finding of the most general interest may be the fact that di-hydrogen molecule can in fact be the stable form of hydrogen in defect-free zirconia. This is a rather unexpected result. Very few studies contemplate indeed the possible stability of H_2 molecules in oxides. Still, a few years ago, H_2 was found stable with a very narrow range of stability in ZnO [34]. Hodille et al. also found molecular hydrogen to be quite stable in BeO [35]. As far as zirconia is concerned, the possibility to have molecular hydrogen has been neglected. It seems however that Youssef et al [36] tackled this possibility. They apparently found that

H₂ can indeed be stable but did not comment any further. In the more specific context of trapping and diffusion of hydrogen in defective zirconia, we find that oxygen vacancies are very effective traps of hydrogen atoms at every temperature. The respective amounts of hydrogen vs oxygen vacancies proves to be the key parameter to control where hydrogen atoms are located in zirconia. The effect of substitutional atoms appears smaller, with an almost negligible effect of Sn and a moderate trapping on Nb.

As far as hydrogen diffusion is concerned, the present study was motivated by our findings that proton diffusion in defect-free zirconia appeared much larger than the actual diffusion of H in zirconia layers. Our suspicion of hydrogen trapping by defects is confirmed by our results with an indication that oxygen vacancies may play a major role in such trapping. Hydrogen diffusion is very likely slowed down by this trapping. It has recently been advocated that H₂ molecule diffusion through nano-pores in the zirconia layer can contribute significantly to the transport of hydrogen [14]. Our finding that molecular hydrogen can be stable in zirconia show that some of these molecules may come from the bulk of zirconia.

Finally, in this work, we showed that there is a change in the most abundant form of hydrogen depending on the hydrogen to oxygen vacancy ratio. Then, due to vacancy concentration gradient through the oxide layer formed on zirconium alloys, hydrogen is likely trapped in this type of defects in the inner part of the oxide scale and is in the molecular form (H₂)_i in the outer part. These species certainly do not diffuse at the same rate. These results thus provide a possible explanation for the variation of hydrogen diffusion coefficient through the oxide layer that is observed experimentally. To actually calculate the effects of trapping on the diffusion coefficient of hydrogen one would need to consider the trapping and de-trapping of hydrogen from the vacancies and the collective diffusion of hydrogen atoms associated with oxygen vacancies. We shall tackle these phenomena in a future.

VI Acknowledgments

This work was partly funded by the project « gaine » of the French I3P. This work was granted access to the HPC resources of CINES under the allocation 2020-A0080910067 attributed by GENCI (Grand Equipement National de Calcul Intensif).

VII References

- [1] J.H. Austin, T.S. Elleman, K. Verghese, Tritium diffusion in zircaloy-2 in the temperature range -78 to 204°C , *J. Nucl. Mater.* 51(3) (1974) 321-329.
- [2] D. Khatamian, F.D. Manchester, An ion beam study of hydrogen diffusion in oxides of Zr and Zr-Nb (2.5 wt%): I. Diffusion parameters for dense oxide, *J. Nucl. Mater.* 166(3) (1989) 300-306.
- [3] D. Khatamian, Diffusion of hydrogen in the oxides of Zr1Nb, Zr2.5Nb and Zr20Nb alloys, *Zeitschrift für Physikalische Chemie*, Bd.181.S.435-440 (1993).
- [4] D. Khatamian, Diffusion of Hydrogen in Single Crystals of Monoclinic-ZrO₂ and Yttrium Stabilized Cubic Zirconia, *Defect Diffus. Forum* 297-301 (2010) 631-640.
- [5] Y. Hatano, R. Hitaka, M. Sugisaki, M. Hayashi, Transport mechanism of hydrogen through oxide film formed on zircaloy-4, *Journal of Radioanalytical and Nuclear Chemistry* 239(3) (1999) 445-448.
- [6] W. Kunz, H. Münzel, U. Kunz, Tritium release from Zircaloy-2: Dependence on temperature, surface conditions and composition of surrounding medium, *J. Nucl. Mater.* 136(1) (1985) 6-15.
- [7] M. Tupin, F. Martin, C. Bisor, R. Verlet, P. Bossis, J. Chene, F. Jomard, P. Berger, S. Pascal, N. Nuns, Hydrogen diffusion process in the oxides formed on zirconium alloys during corrosion in pressurized water reactor conditions, *Corrosion Science* 116 (2017) 1-13.
- [8] D. Khatamian, Hydrogen diffusion in oxides formed on surfaces of zirconium alloys, *Journal of Alloys and Compounds* 253-254 (1997) 471-474.
- [9] I. Takagi, K. Une, S. Miyamura, T. Kobayashi, Deuterium diffusion in steam-corroded oxide layer of zirconium alloys, *J. Nucl. Mater.* 419(1-3) (2011) 339-346.
- [10] L. Afore, Etude du transport de l'hydrogène produit lors de la corrosion des gaines d'éléments combustibles des réacteurs à eau sous pression dans la zircone et le Zircaloy-4, Aix-Marseille 2 University 1997.
- [11] G. Sundell, M. Thuvander, A.K. Yatim, H. Nordin, H.O. Andrén, Direct observation of hydrogen and deuterium in oxide grain boundaries in corroded Zirconium alloys, *Corrosion Science* 90 (2015) 1-4.
- [12] B. Queylat, Compréhension de l'évolution de la fraction d'hydrogène absorbé par les gaines en alliage de zirconium, École Normale Supérieure Paris-Saclay, 2020, p. 219.
- [13] M. Jublot, G. Zumpicchiati, M. Tupin, S. Pascal, C. Berdin, C. Bisor, M. Blat-Yrieix, Influence of Hydride Precipitation on the Corrosion Kinetics of Zircaloy-4: Effect of the Nanostructure and Grain Boundary Properties of the Zirconium Oxide Layer on Oxygen Diffusion Flux, in: R. Comstock, A. Motta (Eds.), *ASTM International*, West Conshohocken, PA, 2018, pp. 350-384.
- [14] J. Hu, J. Liu, S. Lozano-Perez, C.R.M. Grovenor, M. Christensen, W. Wolf, E. Wimmer, E.V. Mader, Hydrogen pickup during oxidation in aqueous environments: The role of nano-pores and nano-pipes in zirconium oxide films, *Acta Mater.* 180 (2019) 105-115.
- [15] A. Couet, L. Borrel, J. Liu, J. Hu, C. Grovenor, An integrated modeling and experimental approach to study hydrogen pickup mechanism in zirconium alloys, *Corrosion Science* 159 (2019).
- [16] O. Barbour, J.P. Crocombette, T. Schuler, M. Tupin, Ab-initio calculations of hydrogen diffusion coefficient in monoclinic zirconia, *J. Nucl. Mater.* 539 (2020) 152333.
- [17] G. Kresse, J. Furthmüller, Efficient iterative schemes for ab initio total-energy calculations using a plane-wave basis set, *Phys. Rev. B* 54(16) (1996) 11169-11186.
- [18] G. Kresse, D. Joubert, From ultrasoft pseudopotentials to the projector augmented-wave method, *Phys. Rev. B* 59(3) (1999) 1758-1775.
- [19] P.E. Blochl, Projector Augmented-Wave Method, *Phys. Rev. B* 50(24) (1994) 17953-17979.
- [20] J.P. Perdew, K. Burke, M. Ernzerhof, Generalized gradient approximation made simple, *Physical Review Letters* 77 (1996) 3865.
- [21] J. Heyd, G.E. Scuseria, M. Ernzerhof, Hybrid functionals based on a screened Coulomb potential (vol 118, pg 8207, 2003), *J. Chem. Phys.* 124(21) (2006) 219906.
- [22] S.E. Taylor, F. Bruneval, Understanding and correcting the spurious interactions in charged supercells, *Phys. Rev. B* 84(7) (2011) 075155.

- [23] P.J. Harrop, J.N. Wanklyn, The dielectric constant of zirconia, *British Journal of Applied Physics* 18(6) (1967) 739-742.
- [24] B.D.C. Bell, S.T. Murphy, R.W. Grimes, M.R. Wenman, The effect of Nb on the corrosion and hydrogen pick-up of Zr alloys, *Acta Mater.* 132 (2017) 425-431.
- [25] P. Bossis, J. Thomazet, F. Lefebvre, Study of the mechanisms controlling the oxide growth under irradiation: Characterization of irradiated zircaloy-4 and Zr-1Nb-O oxide scales, *ASTM Special Technical Publication*, 2002, pp. 190-217.
- [26] M. Tupin, R. Verlet, K. Wolski, S. Miro, G. Baldacchino, M. Jublot, K. Colas, P. Bossis, A. Ambard, D. Kaczorowski, M. Blat-Yrieix, I. Idarraga, Understanding of corrosion mechanisms after irradiation: Effect of ion irradiation of the oxide layers on the corrosion rate of M5, *ASTM Special Technical Publication*, 2018, pp. 415-447.
- [27] M. Moorehead, Z. Yu, L. Borrel, J. Hu, Z. Cai, A. Couet, Comprehensive investigation of the role of Nb on the oxidation kinetics of Zr-Nb alloys, *Corrosion Science* 155 (2019) 173-181.
- [28] D. Pêcheur, V.R. Filippov, A.B. Bateev, J.J. Ivanov, Mössbauer investigations of the chemical states of tin and iron atoms in zirconium alloy oxide film, *ASTM Special Technical Publication*, 2002, pp. 135-151.
- [29] H.J. Matzke, *Canadian Report AECL-2585* (1966).
- [30] J.P. Crocombette, First-principles study with charge effects of the incorporation of iodine in UO₂, *J. Nucl. Mater.* 429(1-3) (2012) 70-77.
- [31] A. Couet, A.T. Motta, A. Ambard, The coupled current charge compensation model for zirconium alloy fuel cladding oxidation: I. Parabolic oxidation of zirconium alloys, *Corrosion Science* 100 (2015) 73-84.
- [32] P. Barberis, D. Charquet, V. Rebeyrolle, Ternary Zr–Nb–Fe(O) system: phase diagram at 853 K and corrosion behaviour in the domain Nb<0.8%, *J. Nucl. Mater.* 326(2-3) (2004) 163-174.
- [33] Scipy, scipy. <https://www.scipy.org/>.
- [34] C.G. Van De Walle, Hydrogen as a cause of doping in zinc oxide, *Physical Review Letters* 85(5) (2000) 1012-1015.
- [35] E.A. Hodille, Y. Ferro, Z.A. Piazza, C. Pardanaud, Hydrogen in beryllium oxide investigated by DFT: On the relative stability of charged-state atomic versus molecular hydrogen, *Journal of Physics Condensed Matter* 30(30) (2018).
- [36] M. Youssef, B. Yildiz, Hydrogen defects in tetragonal ZrO₂ studied using density functional theory, *Physical Chemistry Chemical Physics* 16(4) (2014) 1354-1365.

